Journal Pre-proofs

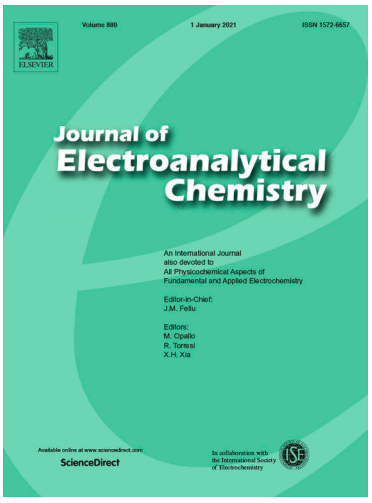

TiO_2 nanotube arrays grown in ethylene glycol-based media containing fluoride: Understanding the effect of early anodization stages on the morphology

Martín I. Broens, Wilkendry Ramos Cervantes, Andrés M. Asenjo Collao, Rodrigo A. Iglesias, Manuel López Teijelo, Omar E. Linarez Pérez

PII: S1572-6657(23)00174-1
DOI: https://doi.org/10.1016/j.jelechem.2023.117314
Reference: JEAC 117314

To appear in: *Journal of Electroanalytical Chemistry*

Received Date: 7 February 2023
Revised Date: 5 March 2023
Accepted Date: 7 March 2023

Please cite this article as: M.I. Broens, W.R. Cervantes, M.A. Collao, R.A. Iglesias, M.L. Teijelo, O.E. Linarez Pérez, TiO_2 nanotube arrays grown in ethylene glycol-based media containing fluoride: Understanding the effect of early anodization stages on the morphology, *Journal of Electroanalytical Chemistry* (2023), doi: https://doi.org/10.1016/j.jelechem.2023.117314

TiO_2 nanotube arrays grown in ethylene glycol-based media containing fluoride: Understanding the effect of early anodization stages on the morphology.

Martín I. Broens[1,2], Wilkendry Ramos Cervantes[1,2], Andrés M. Asenjo Collao[1,2], Rodrigo A. Iglesias[1,2], Manuel López Teijelo[1,*], Omar E. Linarez Pérez[1,2,*]

[1]Universidad Nacional de Córdoba, Facultad de Ciencias Químicas, Departamento de Fisicoquímica, Haya de la Torre esq. Medina Allende, X5000HUA, Córdoba, Argentina.

[2]CONICET, INFIQC, Haya de la Torre esq. Medina Allende, X5000HUA, Córdoba, Argentina.

(*) Corresponding authors:

M. López Teijelo (mlopezteijelo@gmail.com)

O. E. Linarez Pérez (olinarez@unc.edu.ar)

Abstract

In this work, we develop a phenomenological model describing the growth of TiO_2 nanotube arrays (NTA-TiO_2) by titanium anodization in ethylene glycol-based electrolytes containing fluoride. NTA-TiO_2 formation is described in terms of the well-known High-Field mechanism (HFM) considering film thinning by dissolution, and the electronic current contribution according to the Oxygen Bubble Mold (OBM) model, as it has been previously reported. For the first time, the inclusion of the nucleation of oxygen bubbles as the rate determining step at early anodization times is considered. By simultaneous fitting of the potentiostatic j/t profiles and the time evolution of morphological features such as pore radius, layer thickness and density of pores, the behavior observed for several experimental conditions is accurately described, in contrast to previously reported Field Assisted Dissolution (FAD) and OBM models. Proposed model allows obtaining physical and phenomenological information concerning the formation and growth of nanoporous oxide films as well as their morphological properties. Results also indicate that fluoride species play a key role at the early anodization stages, determining the subsequent film morphology evolution. Also, conclusive evidence for a chemical-type instead of field-assisted film dissolution process is obtained.

Keywords: Pore nucleation, nanoporous oxide films, electron avalanche, chemical film dissolution

1. Introduction

The knowledge of the mechanisms involved in the growth of solid phases such as thin films, multilayers, (nano)particles and composite materials on different substrates, plays a key role in the control and design of new nanoarchitectures. To obtain these structures, several synthesis methods including electrochemical routes have been reported, which stands out as relatively simple procedures to achieve reproducible and accurately controlled dimensions as well as interesting morphological features [1-6]. Particularly, the anodization of Ti, under specific experimental conditions, leading to the generation of self-organized TiO_2 nanotube arrays (NTA-TiO_2) is widely known for their revamped applications in several fields [4-26]. During the anodization process of Ti under potentiostatic or galvanostatic conditions, distinct stages are observed in the current- or potential- time response, respectively, which are commonly correlated to the controlling processes taking place and the morphological evolution observed in the resulting layers.

In spite of the considerable number of reports on the anodic formation of self-organized NTA-TiO_2, the mechanism controlling the overall process is still under discussion and different models have been proposed to understand oxide nanostructuration [7-28]. Among them, Field-Assisted Dissolution (FAD) and Oxygen Bubble Mold (OBM) models are usually considered separately by most authors in phenomenological interpretations [7,9,10,15-19,27-30]. Scheme 1 shows comparatively the main features of both models. At the first stage of anodization, the growth of a homogeneous TiO_2 barrier layer takes place (Scheme 1a), according to the overall reaction:

$$Ti(s) + 2H_2O(l) \rightarrow TiO_2(s) + 4H^+(aq) + 4e^- \quad (1)$$

Both FAD and OBM models agree that the TiO_2 films grow by ionic migration in terms of the well-known High Field Model (HFM, *ionic current*) [7,9,10,27-32]. However, they state that the porous nature of the film obtained afterwards is produced as a consequence of different processes. Briefly, FAD model assumes that the NTA-TiO_2 are generated by the local film dissolution induced by fluoride ions from the electrolyte at preferential points of the oxide/electrolyte interface. Then, a weakening of Ti-O bonds as a consequence of the high electric field applied leads to form a porous structure (Scheme 1b,c) [7,9,10,29,30], according to the overall chemical reaction:

$$TiO_2(s) + 6F^-(aq) + 4H^+(aq) \rightarrow [TiF_6]^{2-}(aq) + 2H_2O(l) \quad (2)$$

Despite the spontaneous thermodynamic nature of reaction (2) under typical anodizing conditions [8], the field-assisted origin attributed to this reaction is the main controversial feature of the FAD model due mainly to the lack of experimental evidence [15-19]. On the other hand, OBM model assumes that the production of oxygen bubbles inside the oxide phase, due to the formation of a fluoride-rich region near the film/electrolyte interface, is the controlling step to generate the pores, in agreement with:

$$2H_2O(l) \rightarrow O_2(g) + 4H^+(aq) + 4e^- \quad (3)$$

Then, as (3) continuously occurs, an associated *electronic current* flows and the oxygen bubbles grow, acting as molds for the surrounding oxide expansion by a "plastic flow" mechanism (Scheme 1d,e) [4,33-36]. Recently, X. Zhu *et al*. have reported a series of works with the aim of obtaining evidence against the FAD model [15-19,28,37]. In this regard, their analysis and conclusions are focused on the explanation of different

phenomenological results, such as the presence of nanotube "embryos" and cavities in the TiO_2 layer as well as the formation of partly split nanotubes, which are associated with the generation of occluded oxygen bubbles and their subsequent release effects. Nevertheless, the extended meaning of the explanations in terms of the OBM model may result ambitious and even insufficient from a (electro)chemical point of view for most of the cases.

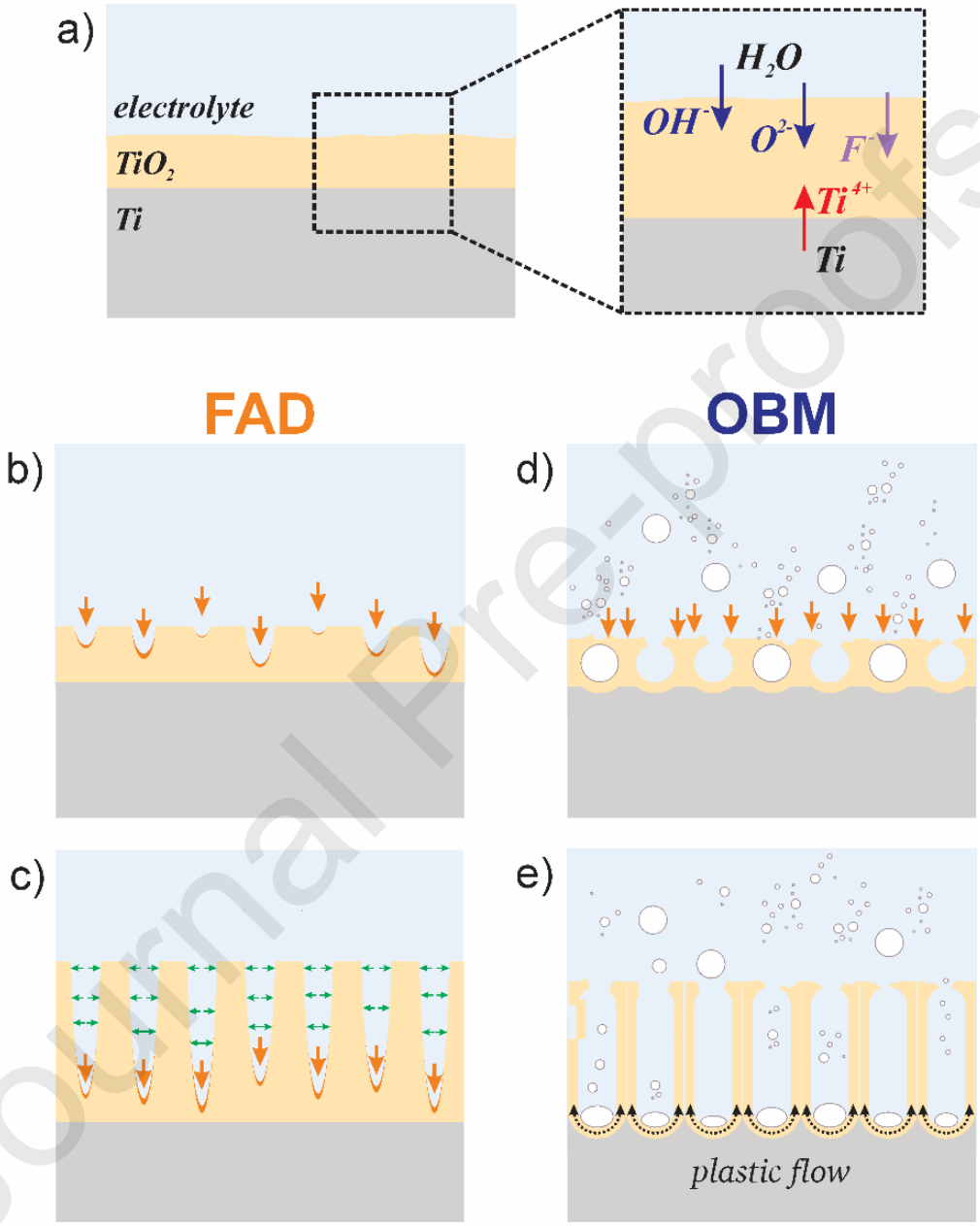

Scheme 1. Comparative schematic representations of FAD and OBM models. Orange and green arrows in b, c and d denote the occurrence of film dissolution according to (2).

Moreover, obtaining TiO_2 layers made of discrete nanotubes instead of integrated nanopores is characteristic of anodizing carried out in fluoride-containing electrolytes. In order to explain this, it has been reported that during anodizing fluoride ions incorporate and transport within the oxide film, leading to the building of a weak anion containing

TiO_2 structure between neighboring pores [5,7,9,10]. This fluoride-rich layer can be easily dissolved by the water contained in the electrolyte, promoting the differentiation into tubes. Alternatively, based on the OBM model, Zhu *et al.* have proposed that the nanotubular nature is given by a radial distribution of the electric field at the pore bottom that promotes the formation of gaps [15].

From the discussion above, in this work we propose a phenomenological model describing the growth of NTA-TiO_2 by titanium anodization in ethylene glycol-based electrolytes containing fluoride. For simplicity this model assumes a nanoporous structure as an approach to the NTA-TiO_2 morphology. The model also considers ionic film growth in terms of the HFM, electronic current contribution according to the OBM model and layer thinning by chemical dissolution. The inclusion of nucleation of oxygen bubbles at early anodization times as the porous layer initiation step takes place, is made for the first time (see below). In addition, this work is the first report that allows obtaining an accurate overall description of both current/time and morphological features evolution during the NTA-TiO_2 growth for several experimental conditions. The present work represents a novel contribution to the understanding of the mechanisms involved in the growth of anodic nanoporous/nanotubular layers and could be of great interest from both fundamental and practical perspectives.

2. Experimental section

Titanium anodization was performed in a jacketed electrochemical cell with a two-electrode configuration. Polycrystalline titanium foils (Alfa Aesar, 99.99+% purity and 127 μm in thickness) mounted on Teflon holders with an exposed geometric area of 0.5 cm^2 were employed as anode, while a titanium sheet (Johnson Matthey Electronics, 99.7% purity and 890 μm in thickness) of 10.5 cm^2 geometric area was used as cathode. Prior to anodization, the electrodes were pretreated first with emery paper abrasion, followed by mechanically polish using 0.1 and 0.05 μm alumina aqueous suspensions on Microcloth (Buehler). After that, the samples were degreased by sonication in a 50:50 acetone/ethanol mixture for 30 min, rinsed with deionized water and dried under N_2 flux. High-voltage anodization experiments were carried out using a 173 EG&G PAR potentiostat/galvanostat (internal power supply of 100 V), coupled to a 175 EG&G PAR signal generator and a 7090A Hewlett Packard plotting recorder. Anodizing electrolyte temperature was set to 5 °C by connecting the cell to a Lauda Alpha cryostat. NTA-TiO_2 growth was performed by direct anodic polarization of the cleaned titanium surfaces by applying a constant voltage step at 5; 10; 20; 30; 40 or 50 V, during different times and with continuous magnetic stirring in order to homogenize the bulk electrolyte temperature and composition. Electrolytic solutions were prepared from analytical grade reagents in ethylene glycol containing 3% V/V water (Milli-Q) and 0.2; 0.4; 0.6 or 0.8% w/V NH_4F.

Top morphology layer features (inner radius, surface distribution, and density of pores/tubes) were characterized by field-emission scanning electron microscopy (FE-SEM) using a Carl Zeiss Σigma microscope, working at 3-5 keV gun power. Layer thickness was determined by tridimensional topography reconstruction using an Olympus LEXT OLS4000 confocal microscope (402 nm laser excitation), as we described previously [38].

Potentiodynamic measurements were performed with a conventional three-electrode cell configuration, using an AUTOLAB PGSTAT100 galvanostat/potentiostat coupled to a voltage multiplier. A platinum sheet of 5 cm^2 and an Ag/AgCl/KCl(sat) electrode were employed as auxiliary and reference electrodes, respectively.

Data fitting and simulation of the potentiostatic j/t profiles, as well as the morphological features dependencies with time, were simultaneously performed by means of the Simplex method and the integration of a proposed set of differential equations (see section SI-1 in Supplementary Information) using the Runge–Kutta algorithm in MATLAB R2020b (MathWorks, Inc.).

3. Results and discussion

3.1. General phenomenology

In this section, the effects of anodization time, applied potential and fluoride concentration on the potentiostatic j/t profile and morphological features of NTA-TiO_2 during the anodization in ethylene glycol-based electrolytes, are discussed. Selected voltage and NH_4F concentration conditions were established according to previous reports, taking in account that oxygen evolution reaction takes place on TiO_2 even at lower potentials (> 1.5 V) [31,39,40] and the water content (3% V/V) as well as the fluoride concentrations employed (0.2-0.8 %w/V NH_4F) allow obtaining NTA-TiO_2 [5,8,9,11,13].

3.1.1. Anodization time

Fig. 1a shows potentiostatic j/t profiles recorded for the anodization of Ti foils at 40 V and 5 ºC in a 0.2% w/V NH_4F + 3% V/V H_2O + ethylene glycol electrolyte. Despite each curve represents a different anodized electrode, very reproducible current profiles are obtained. In addition, Fig. 1b shows top-view FE-SEM images for a non-anodized titanium electrode compared with those of TiO_2 layers obtained after the anodization up to 24 h. Table SI-1a (see Supplementary Information) also summarizes the morphological layer features (inner pore radius, film thickness and pore density) obtained for different anodizing times. In order to get insight the whole anodization process and correlate the final TiO_2 layer morphology with j/t profiles, an estimation of the faradaic efficiency for the NT-TiO_2 growth was performed. For this, the ratio of the measured layer thickness (l in Table S1a) and the estimated theoretical thickness from the recorded current profiles during the anodization time (t_a), assuming that all the anodic charge ($Q = \int_0^{t_a} j dt$) is only due to the TiO_2 film growth process, was considered:

$$faradaic\ efficiency = \frac{l}{\frac{M_{TiO_2}}{zF\rho_{TiO_2}}Q} \quad (4)$$

where M_{TiO_2} and ρ_{TiO_2} are the molar mass and density of bulk TiO_2, respectively, z is the number of electrons involved in the Ti oxidation ($z = 4$ mol e^- per TiO_2 mol), and F is the Faraday constant. Fig. 2a shows comparatively the experimental and theoretical layer

thicknesses, while Fig. 2b shows the faradaic efficiency as a function of the anodization time. Prior to anodizing, Ti surface shows a few morphological features, such as grain boundaries and surface defects due to the material manufacture (Fig. 1b, micrograph labeled as "Ti"). When the voltage step is applied, oxidation of the metallic titanium takes place and very high current densities are obtained (> 1 mA cm^{-2}) (Fig. 1a). Meanwhile, the electrode begins to passivate by the growth of a TiO_2 barrier layer according to reaction (1), which is clearly evidenced from significant changes in surface texture (Fig. 1b, 1- and 15-min) that correlates with an exponential current decrease (Fig. 1a, zone I). Furthermore, a gradual diminishing of the faradaic efficiency is obtained until reaching a minimum value of ~0.5 at around 15 min (Fig. 2b), indicating that other processes are taking place and control the overall current response. Afterwards, the current increases again and defines a maximum (Fig. 1a, zone II), which time (t_m) and current (j_m) values are dependent on the experimental conditions employed (see below). During this time, the electrode surface begins to show pits or cavities with almost circular shape that grow in number and diameter with anodizing extension (Fig. 1b, 30 min to 3 h). Even though TiO_2 layers exhibit a nanoporous appearance from the top-view, a discrete nanotube-formed structure underlies the porous surface layer, which corresponds to the barrier layer formed at early anodization stages (Fig. S1 in Supplementary Information). Moreover, the faradaic efficiency increases again up to almost unity after several hours (t < 6 h), while the layer thickness shows a linear evolution with time (Fig. 2a).

Finally, at more extended anodization times (> 6 h), the current slowly decreases (Fig. 1a, zone III) and a porous to tubular structure evolution is observed due to the complete dissolution of the surface porous layer (Fig. 1b, 12- and 24-h). At this stage, the faradaic efficiency continuously drops to ~0.3 after the continuous anodization up to 24 h, and a nearly constant layer thickness is obtained (Fig. 2a). This drop may result from possible structural and physicochemical changes in the barrier layer that become important with the anodization time and has been disused in previous reports. In order to sustain the growth of the nanotubes, Regonini *et al*. stated the importance of the barrier layer in terms of their thickness and ionic conductivity [8]. In relation to this, some authors have suggested that ionic transport through the barrier layer is negatively affected by the continuous incorporation of fluoride, carbon species, and hydroxyl ions during the anodization [8,41]. Also, chemical etching of the tubes mouth takes place for long-time exposure to the electrolyte, especially in conditions with high fluoride concentration, low water content or highly viscous media, leading to lower tube lengths than expected [5,7,9,27,42]. In this regard, also the inner tube shape depends on the anodization conditions. Previously, we demonstrated that water content and anodization medium viscosity affect directly the oxide film dissolution rate generating a more homogeneous concentration gradient of fluoride along the tubes [5]. This effect clearly produces both nanograss-free surfaces and a "V"- to "U"-inner cavity shape transition along the tube as the water content is increased.

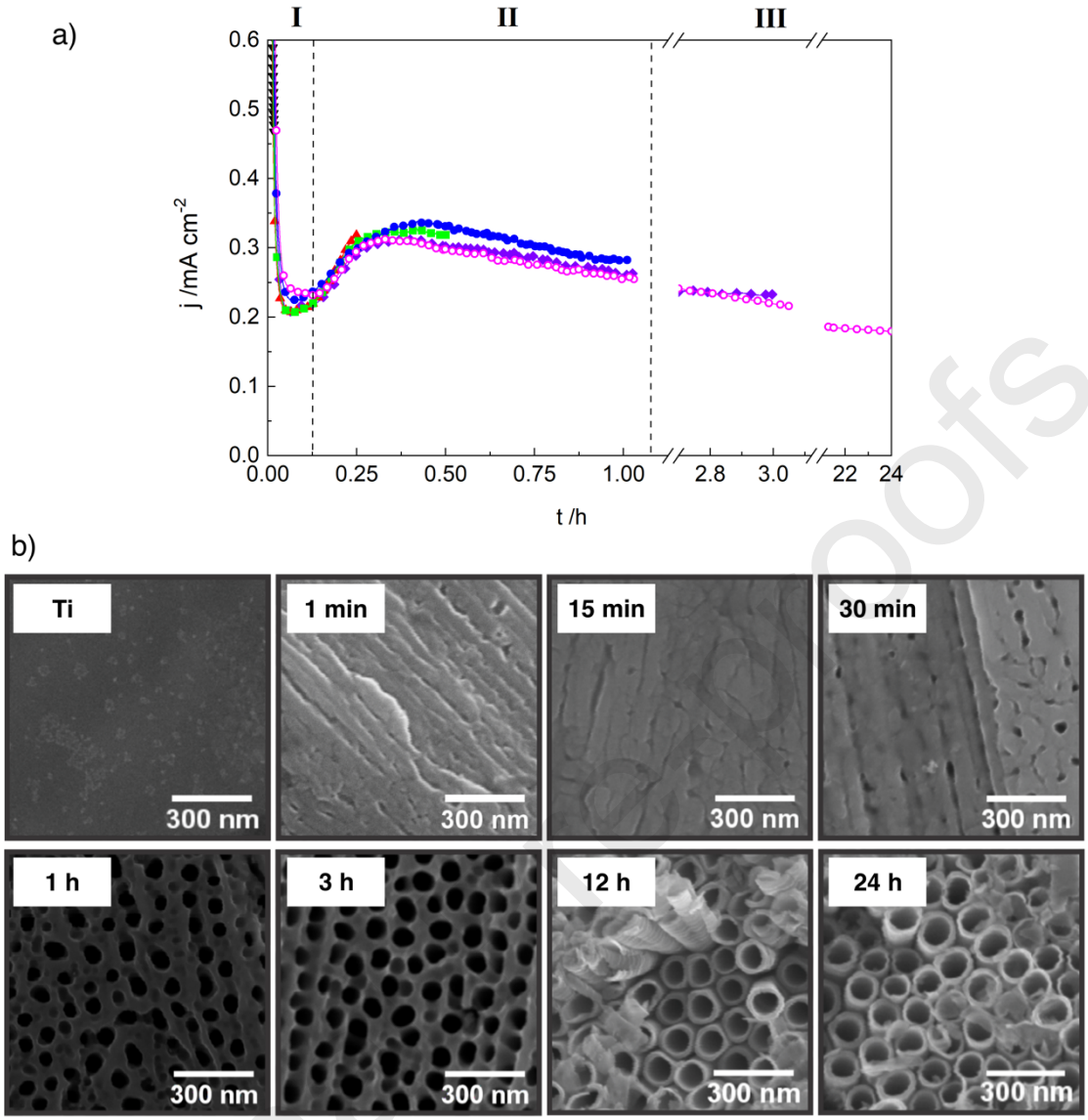

Fig. 1. a) Potentiostatic j/t profiles recorded at 5 ºC for the anodization of Ti foils by applying a voltage step of 40 V in a 0.2% w/V NH_4F + 3% V/V H_2O ethylene glycol electrolyte during different times: 1 min (–▼–); 15 min (–▲–); 30 min (–■–); 1 h (–●–); 3 h (–◆–) and 24 h (–○–). b) Top-view FE-SEM images for a cleaned titanium foil and TiO_2 layers obtained after the anodization up to 24 h.

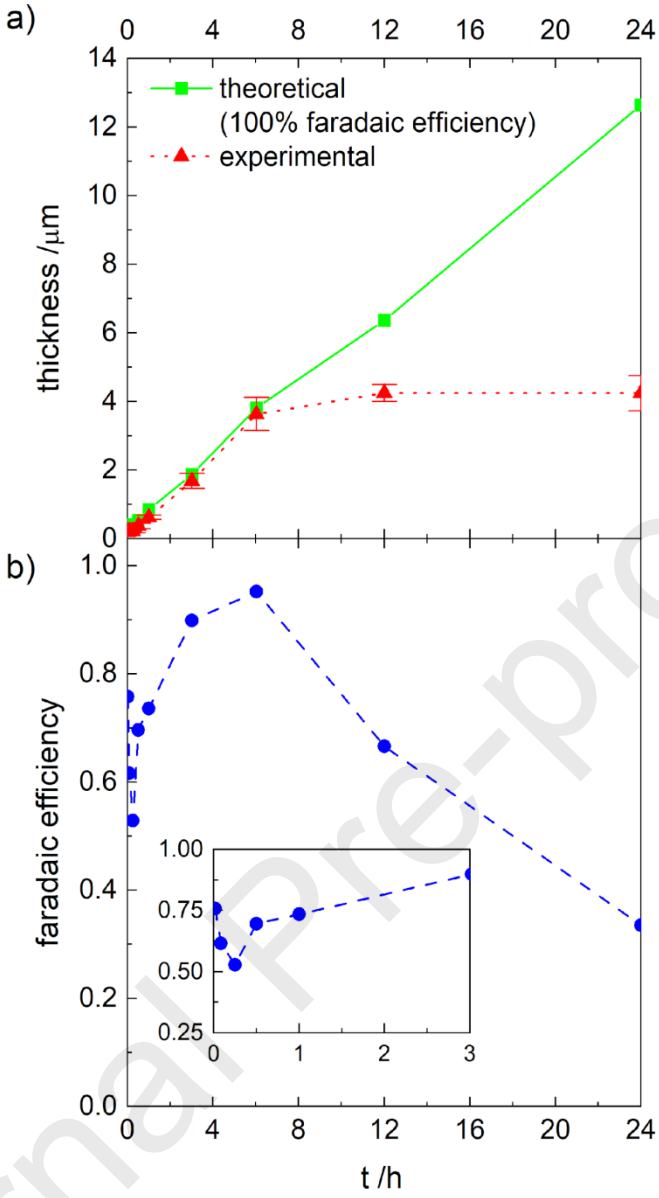

Fig. 2. Time variations of the experimental (–▲–) and theoretical layers thicknesses estimated from the total anodization charge (–■–) (a), and the faradaic efficiency (b) for anodized Ti foils shown in Fig. 1. Inset in b shows the early anodization times at a magnified scale.

3.1.2. Applied voltage

Fig. 3 shows potentiostatic j/t profiles (a) and top-view FE-SEM images (b) for Ti foils anodized during 6 h in a 0.2% w/V NH_4F + ethylene glycol + 3% V/V H_2O electrolytes applying different anodic voltages. An evident nanoporous surface is observed for $E \geq 10$ V, where the pore radius and layer thickness depend on the applied voltage (Fig. 3b and Table SI-1b-d in Supplementary Information). It is worth noting that main changes in current profiles are observed at the first stages of anodization ($t < 30$ min), where the local maximum value of the current (j_m) and its time (t_m) are given by

the experimental conditions. Particularly, as the applied voltage is increased the current profile shape, as well as j_m and t_m values, show a similar behavior to those observed during nucleation processes at metallic or polymeric films electrodeposition [43].

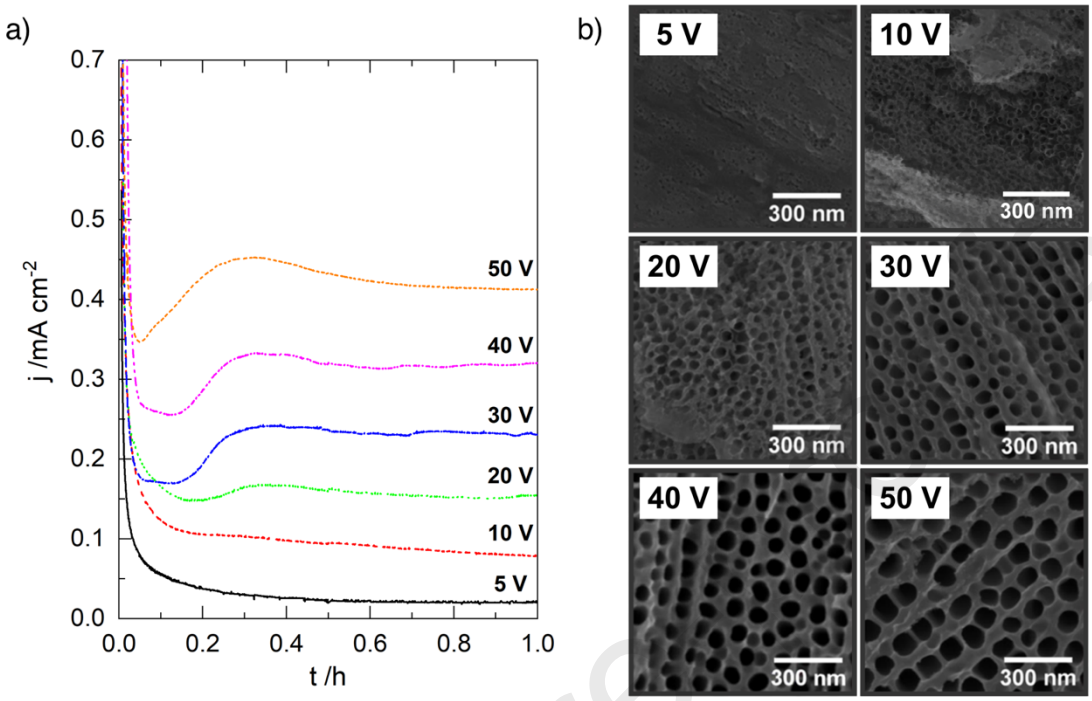

Fig. 3. a) Potentiostatic j/t profiles recorded during the anodizing of Ti foils at 5 ºC for 6 h in 0.2% w/V NH_4F + ethylene glycol + 3% V/V H_2O electrolyte. Applied voltage: 5 V (——); 10 V (– – –); 20 V (•••••); 30 V (– • – •); 40 V (–••–) and 50 V (-----). b) Top-view FE-SEM images for the TiO_2 layers obtained after 6 h polarization.

One of the main controversial statements of the FAD model is the limited proof that field-assisted dissolution is the determinant factor causing the pores formation and growth [15-19,28]. To obtain experimental evidence of this process, repetitive triangular potential sweeps with increasingly anodic switching potentials were performed. Fig. 4 shows the potentiodynamic j/E response obtained at 0.02 V s^{-1} during the anodization of Ti foils up to 7 V (Fig. 4a and b) and 60 V (Fig. 4c) in a 0.2% w/V NH_4F + 3% V/V H_2O + ethylene glycol electrolyte at 5 ºC. According to HFM [25-30], each cycle should show an initial increase of the anodic current until reaching a steady-state value (j_{ss}) as potential is increased, remaining nearly constant in a broad potential range due to the TiO_2 layer thickening. First cycle in Fig. 4a shows this behavior defining a j_{ss} ~16 µA cm^{-2} value up to $E \sim 0.8$ V, and after that the current begins to increase again. When sweep direction is reversed, current decreases as the electric field is lowered due to the almost constant layer thickness previously obtained. For subsequent cycles, no appreciable current flow is observed until reaching a potential near to the switching value of the previous cycle. However, as the switching potentials used in Fig. 4 are close, the j/E shapes recorded do not properly develop the j_{ss} value for all cycles. Also, higher current values are obtained for $E > 1$ V, which is usually attributed to the occurrence of the oxygen evolution reaction jointly with oxide film growth [27-31,39,40,44]. Furthermore, slight curve-crossings for

potentials higher than 5 V are obtained. The increase of the current at a lower potential than the switching value of the previous cycle, seen as a curve-crossing, is direct evidence that some part of the oxide has been dissolved (i.e., the layer has a lower thickness than the one grown in the previous cycle) [30-32]. In addition, the behavior is more marked when the potential is hold at the open circuit value ($E \sim -0.25$ V) during 60 min between successive cycles (Fig. 4b) or the switching potential is increased, indicating the growing importance of the oxide dissolution process with the anodization time. On the other hand, for repetitive sweeps up to potentials higher than 10 V, no appreciable increase of curve-crossing is observed (Fig. 4c). Therefore, these results are strong evidence that the film dissolution promoted by the fluoride ions, according to reaction (2), takes place at a non-negligible rate. As a matter conservative condition must be established at steady state [31], dissolution current (j_{dis}) cannot be higher than the ionic current for the experimental conditions employed (j_{dis}<16 μA cm^{-2}). In turn, this suggests that oxide dissolution is not strong enough to determine the porous nature of the growing film, even though it may be important for the differentiation into nanotubes as well as for nanograss formation when anodization time increases [5,9,27,28,42].

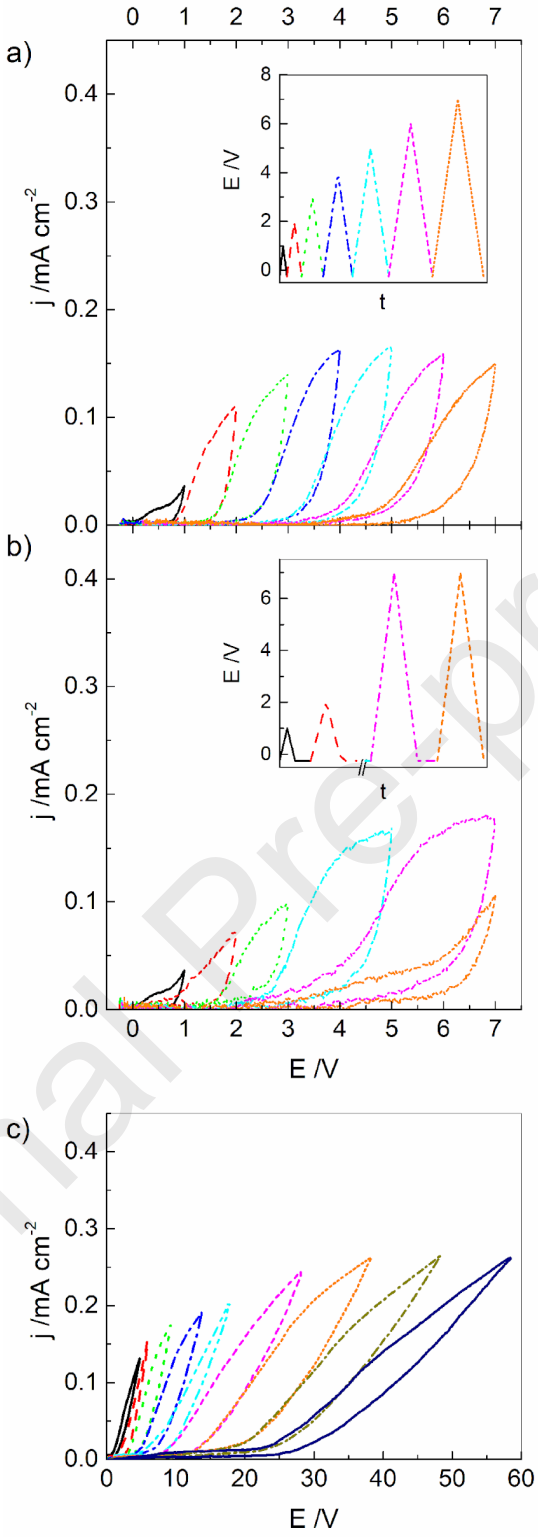

Fig. 4. Potentiodynamic j/E profiles recorded at 0.02 V s^{-1} for the anodization of Ti foils in a 0.2% w/V NH_4F + 3% V/V H_2O + ethylene glycol electrolyte at 5 ºC, applying repetitive potential sweeps with increasing anodic switching potentials up to 7 V (a and b) or 60 V (c). Cycles were applied with (b) and without (a and c) open circuit potential holdings during 60 min between each cycle. Insets show E/t programs applied.

3.1.3. Fluoride concentration

Fig. 5 shows potentiostatic j/t profiles recorded for the anodization of Ti foils at 40 V and 5 ºC in a 3% V/V H_2O + 97% V/V ethylene glycol electrolyte with different fluoride contents. Similarly to applied voltage effect (Fig. 3a), strong dependencies of the current profiles and surface morphology of the NTA-TiO_2 are observed. A noticeable dependence on fluoride concentration of the surface appearance obtained from top-view images as either pores or discrete nanotubes, is obtained. In addition, as the fluoride content is increased, j_m and t_m values show a marked trend in comparison to the observed as applied voltage is increased (i.e. j_m increases and t_m decreases as fluoride concentration is augmented, see Fig. 3), indicating a strong dependence of subsequent nanotubular evolution with the fluoride content in the electrolyte.

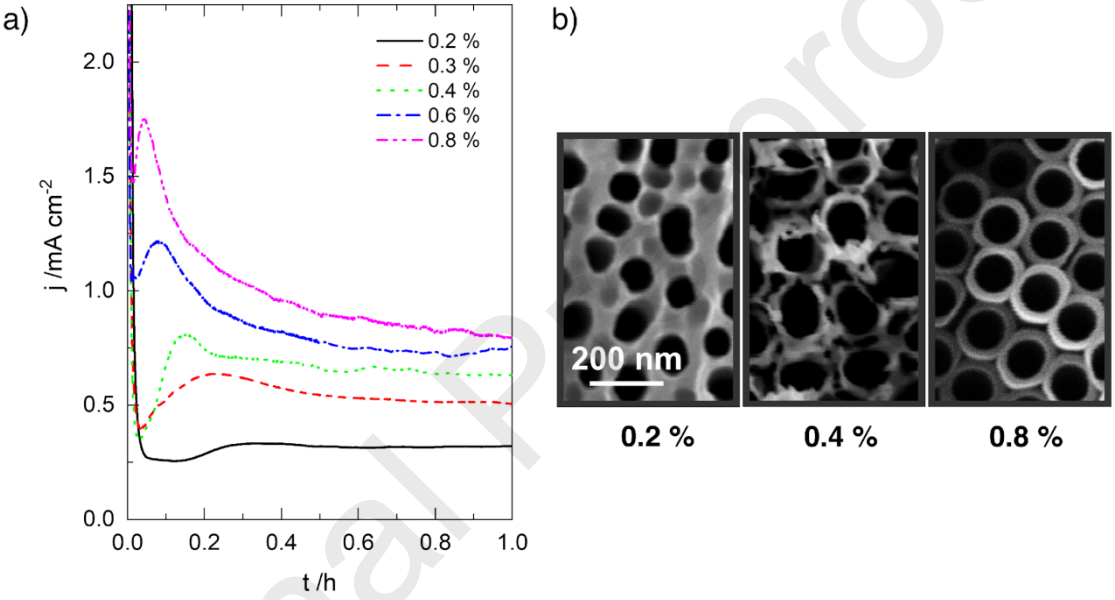

Fig. 5. Potentiostatic j/t profiles (a) and top-view FE-SEM images (b) for Ti foils anodized at 40 V during 6 h in 3% V/V H_2O + ethylene glycol electrolyte at 5 ºC for different fluoride concentration: 0.2 (——); 0.3 (– – –); 0.4 (•••••); 0.6 % (– • – •) and 0.8 % w/V (–••–).

In summary, these results showed the usual phenomenology obtained during the titanium anodization in ethylene glycol-based media containing fluoride. A strong dependence of both surface morphology and film quality on the experimental conditions employed (anodization time, voltage applied, and fluoride concentration, among others) is observed. In addition, potentiostatic j/t curves clearly show that first anodization stages play a key role in the evolution of oxide nanostructuration, which is related to the pore nucleation process. Accordingly, this complex behavior can not be completely described either by FAD or OBM models alone.

3.2. Nanoporous film growth model

According to the general sketch shown in Scheme 1a, during titanium anodization the injection of Ti^{4+} ions from the metallic electrode at the Ti/TiO_2 interface takes place simultaneously with the incorporation of oxide (and hydroxyl) anions from the water content in the electrolyte at the TiO_2/electrolyte interface. Consequently, the migration of Ti^{4+} and O^{2-} species within the oxide phase gives rise to the formation and growth of the TiO_2 film, according to reaction (1). Usually, the ionic current (j_{HFM}) for film growth is described in terms of the HFM [7,9,29-32]:

$$j_{HFM} = Aexp(\beta\epsilon) \quad (5)$$

where A and β are parameters that depend on the microscopic oxide properties, as well as temperature, and ϵ is the electric field ($\epsilon = \frac{E}{d_b}$) determined by the potential drop (E) inside the barrier oxide film of thickness d_b. According to the faradaic mass balance, the thickness increases as:

$$d_b(t) = d_o + \frac{M_{TiO_2}}{zF\rho_{TiO_2}}\int_0^t (j_{HFM} - j_{dis})dt \quad (6)$$

where d_o is the initial oxide thickness. Also, the constant term j_{dis} in (6) represents the current associated with the loss of charge due to oxide thickness diminishing by dissolution during film growth [32] (see section 3.1.2).

Simultaneously with the film growth, fluoride incorporation into the oxide phase may also take place at the TiO_2/electrolyte interface, $F^-(electrolyte) \rightarrow F^-(oxide)$ [29-32,44]. Then, incorporated $F^-(oxide)$ species can act as impurity centers generating surface levels within the oxide band gap, which can release electrons by tunneling to the semiconductor conduction band (CB) defining an initial electronic contribution ($j_{e,o}$), $F^-(oxide) \rightarrow F(oxide) + e^-(CB)$ [4,15-20,38,45,46]. As a result of the high electric field applied, electrons are accelerated and multiplied in avalanche across the film until reaching the underneath titanium substrate, producing an exponential increase of the electronic current (j_{elec}) as the barrier layer thickness increases according to the theory of electron avalanche proposed by Albella *et al.* [46]:

$$j_{elec} = j_{e,o}exp\ (\alpha d_b) \quad (7)$$

where α is the impact ionization factor coefficient (inverse of the electron mean free path, ~10^5 cm^{-1}).

On the other hand, the high values of voltages usually employed (E > 1.5 V, see section 3.1) for titanium anodization in ethylene glycol-based electrolytes represent high enough overpotentials for the oxygen evolution reaction (OER) to occur. Consequently, the electron avalanche is catalyzed by the ionized incorporated fluoride that behaves as avid electron centers, which restore their charge through the OER according to

$$2O^{2-}(oxide) + 4F(oxide) \rightarrow O_2(g,bubble) + 4F^-(oxide) \quad (8)$$

Then, the occluded oxygen bubbles grow and expand upwards, acting as physical hindrances that promote the development of pores by the plastic flow of the surrounding

growing oxide (see Scheme 1e). Assuming that mainly fluoride ions diffusion inside the film determines the nucleation and growth of oxygen bubbles, with a cylindrical shape, and the overlapping of the diffusional zones in an extended fraction area (f_d) may take place [42,47-49], the charge related to the nucleation of pore embryos can be described as a nucleation current (j_{nuc}), conforming to [49]:

$$j_{nuc} = zFc_F\frac{D}{\sqrt{\pi Dt}}f_d(t) \quad (9)$$

where c_F and D are the concentration and diffusion coefficient of the fluoride ions inside the TiO_2 layer, respectively. According to the Avrami theorem, for a random and homogeneous nucleation of N_{max} diffusion nucleus with radius r_d, the fraction f_d is defined as [47-50]:

$$f_d(t) = 1 - exp\left[-N_{max}\pi r_d(t)^2\right] \quad (10)$$

Sections SI-2 and SI-3 in Supplementary Information show that the diffusion radius is determined by the geometrical bubble radius (r_o) that, in turn, can be obtained assuming the simultaneous growth in length (l) of bubbles with cylindrical shape as:

$$\frac{dr_o}{dt} = \frac{1}{2l(t)}\left(\frac{c_F D M_{O_2}}{\rho_{O_2}} - r_o(t)\frac{dl}{dt}\right) \quad (11)$$

where M_{O_2} and $\rho_{O_2}$are the molar mass and the density of the oxygen bubbles, respectively.

In addition, as anodization time elapses the number and density of bubbles (N_p) increases with a constant formation rate, v_{nuc}, until reaching a maximum value (N_{max}), but also a fraction of neighbor bubbles can coalesce (ηN_{max}) at a v_{coal} rate. Then, a lower number of bubbles survives and evolve to form observable pores in the film, according to [47-49]:

$$N_p(t) = N_{max}(1 - exp[-v_{nuc}t]) - \eta N_{max}(1 - exp[-v_{coal}t]) \quad (12)$$

Overall, the total current density (j) consists in the sum of the ionic current due to the TiO_2 growth according to HFM (j_{HFM}), the dissolution current (j_{dis}), the electronic current due to electron avalanche promoted by fluoride incorporation into the oxide lattice (j_{elec}) and the pore embryos nucleation current of oxygen bubbles assisted by fluoride diffusion inside the film (j_{nuc}):

$$j = j_{HFM} + j_{dis} + j_{elec} + j_{nuc} \quad (13)$$

Note that the $j_{HFM} + j_{dis}$ terms take in account the overall oxide growth charge considering both the net and loss thicknesses, respectively.

3.3. Applicability of the model

Fig. 6 shows the experimental and simulated potentiostatic j/t response recorded at 5 ºC for the anodization of a Ti foil at 40 V during 6 h in a 0.2% w/V NH_4F + 3% V/V

H_2O + ethylene glycol electrolyte. In addition, simulated j/t curves for the ionic, dissolution, electronic and nucleation current contributions are also shown. Curve fitting was performed assuming that the nanotubular structure can be approximated to a nanoporous layer (as previously mentioned) and cylindrical bubble geometrical parameters (r_o and l) are representative of the pore radius and the layer thickness, respectively. In addition, according to previous reports [4-20] and our observations (Table SI-1), a constant rate for the layer thickness growth is assumed ($\frac{dl}{dt} = \sigma$). Additionally, Table 1a summarizes the values of the resulting fitting parameters. A very good correlation between experimental and simulated curves is obtained, even for anodization times up to 6 h. Furthermore, it is clearly seen that at the first anodization steps, the nucleation process represents a substantial contribution to the total current compared with both ionic and electronic contributions. In addition, the maximum current value and its position are adequately reproduced by the j_{nuc} contribution. To the best of our knowledge, this is the first report that properly describes these observations, in contrast to the commonly employed FAD and OBM models. From these results, the anodization of titanium in ethylene glycol-based electrolytes containing fluoride can be summarized as follows. When an elevated potential is applied, the high electrical field generates a barrier TiO_2 layer, which grows by ion migration mechanism (i.e. according to the HFM). Simultaneously, the incorporation of fluoride inside the oxide takes place and, consequently, a random distribution of oxygen bubble embryos begins to nucleate and grow according to a fluoride diffusional control. Meanwhile, the density of oxygen bubbles rapidly increases, and their coalescence leads to an observable density of pores at the oxide surface, which grow radial and longitudinally as the TiO_2 continuously develop around the gas bubbles by a plastic flow mechanism.

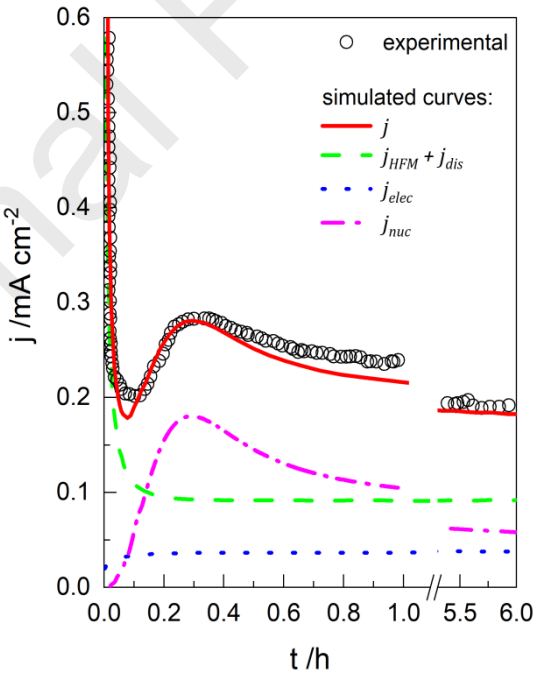

Fig. 6. Experimental potentiostatic j/t profile recorded at 5 ºC for the anodization at 40 V of Ti foils during 6 h in a 0.2% w/V NH_4F + 3% V/V H_2O + ethylene glycol electrolyte (●). Lines represent the simulated curves for the total current j (——); ionic and

dissolution $j_{HFM} + j_{dis}$ (– – –); electronic j_{elec} (⋯⋯) and nucleation j_{nuc} (–·–·–) current contributions. Simulation parameters are listed in Table 1.

In addition, Fig. 7 shows experimental radius, layer thickness and pore density obtained for different anodization times (up to 24 h) as compared with simulated values, and a schematic representation of top- and lateral-views of a nanopore. Accurate description of experimental data is obtained for the radius in the entire anodization time range studied, while the film thickness is overestimated for long anodization times (> 6 h) according to the drop in faradaic efficiency observed in Fig. 2b, which is in good agreement with previous reports [41,51,52]. Due to the complexity of the Ti anodization in ethylene glycol media, the effect of other known processes taking place (i.e., changes in ionic conductivity, chemical etching, tube rupture to form nanograss and non-cylindrical inner tube shapes) were not considered in the present model.

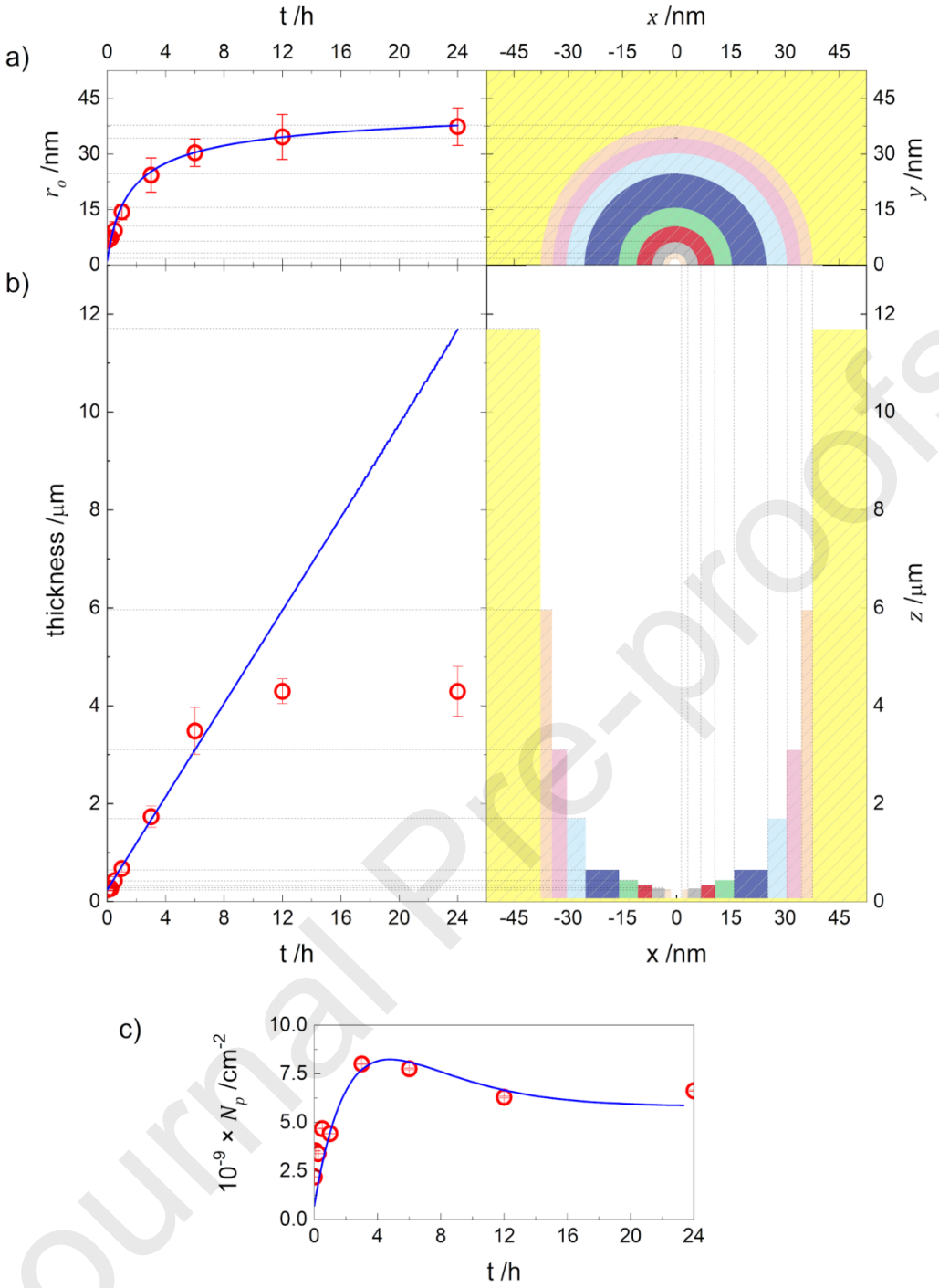

Fig. 7. Measured data (○) and simulated curves (——) for pore radius (a), film thickness (b) and pore density (c). Right side in a and b shows schematic representation of top and cross-section tube evolution. NTA-TiO_2 were grown at 5 ºC by applying a voltage step of 40 V in a 0.2% w/V NH_4F + 3% V/V H_2O ethylene glycol electrolyte during different times.

On the other hand, Supplementary Information shows the best fittings obtained for the potentiostatic j/t response (Fig. S2) and the temporal dependences of r_o, l and N_p (Fig. S3) for NTA-TiO_2 grown in an electrolytic bath containing higher fluoride concentration (0.8% w/V). Table 1b also summarizes the values of the resulting fitting

parameters. For the anodization conditions explored, a good agreement between the simulated and experimental data is obtained for both j/t profiles as well as the morphological parameters up to an anodization time values of 6 h.

According to the estimated fitting parameters (Table 1), no noticeable variations in the oxide growth parameters (A and β) are obtained for the experimental conditions explored. According to HFM,

$$\beta = \frac{qa}{kT} \tag{14}$$

where q is the charge of the main carrier species in the film (q = 2 for oxygen vacancies), $2a$ is the characteristic jump distance between two adjacent positions in the oxide lattice, and kT has the usual meaning. Therefore, the obtained $\beta \sim 3\text{x}10^{-6}$ cm V^{-1} value leads to a $2a$ = 7.7 Å jump distance, which agrees with the average lattice parameter expected for anatase TiO_2 at 298 K [53]. Additionally, significant increases of the initial electronic current near the film/oxide interface ($j_{e,o}$), pore nucleation rate (υ_{nuc}) and fluoride diffusion coefficient (D) are observed when applied voltage and fluoride concentration are increased. The obtained dependences for D (Table 1) indicate that this parameter behaves rather as a transport coefficient, combining the concentration c and the diffusion coefficient D_F of the fluoride ions in the TiO_2 film, as stated in equation (9). For all conditions explored, the ratio $j_{e,o}/j_{ion} < 0.25$ (where j_{ion} is the ionic current estimated at constant electric field conditions) is in good agreement with the expected for TiO_2 growth at voltages lower than the breakdown [46]. Also, fluoride transport coefficient (D) estimated are $\sim 10^{-12}$ cm^2 s^{-1}, which is consistent for ion diffusion inside a solid lattice [54-56].

On the other hand, Table 1b shows an evident dependence of the chemical dissolution rate (j_{dis}) with the fluoride content in opposite to an almost constant j_{dis} value as the applied voltage is increased. These results stand out as conclusive evidence for a chemical-type instead of field-assisted dissolution process promoted by the fluoride ions at a non-negligible constant rate independently of the applied voltage.

In addition, due to the similarity between the diffusional pore nucleation equations (see (9) and (10)) and the usually employed to describe tridimensional nucleation process for metals electrodeposition, an analysis based on reduced variables was performed [47-49]. Fig. 8 shows the non-dimensional $(j_{nuc}/j_{max})^2$ vs t/t_{max} plots for the nucleation current contribution extracted from the fittings of the experimental j/t profiles shown in Figs. 3a and 5a (please note that j_{max} and t_{max} are the local maximum value of the current and its time, respectively, extracted from the j_{nuc} simulated curve). In order to describe the nucleation nature, theoretical profiles for instantaneous and progressive tridimensional nucleation are also included. For different applied voltages and the lowest fluoride content employed (i.e. 0.2% w/V NH4F), an almost pure progressive nucleation of oxygen bubbles embryos is obtained (Fig. 8a). On the other hand, it is evident a gradual variation from a mixed progressive/instantaneous to a purely instantaneous nucleation as fluoride concentration is increased. This indicates that for high-enough fluoride content, all the nuclei are formed and the oxygen bubbles begin to grow as quick as the voltage step is set (t_a = 0). On the contrary, for lower fluoride content, nucleation of embryos slowly takes place until obtaining an enriched fluoride layer which allows the three-dimensional growth of the oxygen bubbles. This behavior is also observed in the variation

of the density of pores at lower times for the fluoride content condition explored (Figs. 7c and S3c). Therefore, fluoride concentration is directly related to the nucleation regimen (i.e., progressive/instantaneous) at early anodization stages which in turn, determines the subsequent nanotubular evolution.

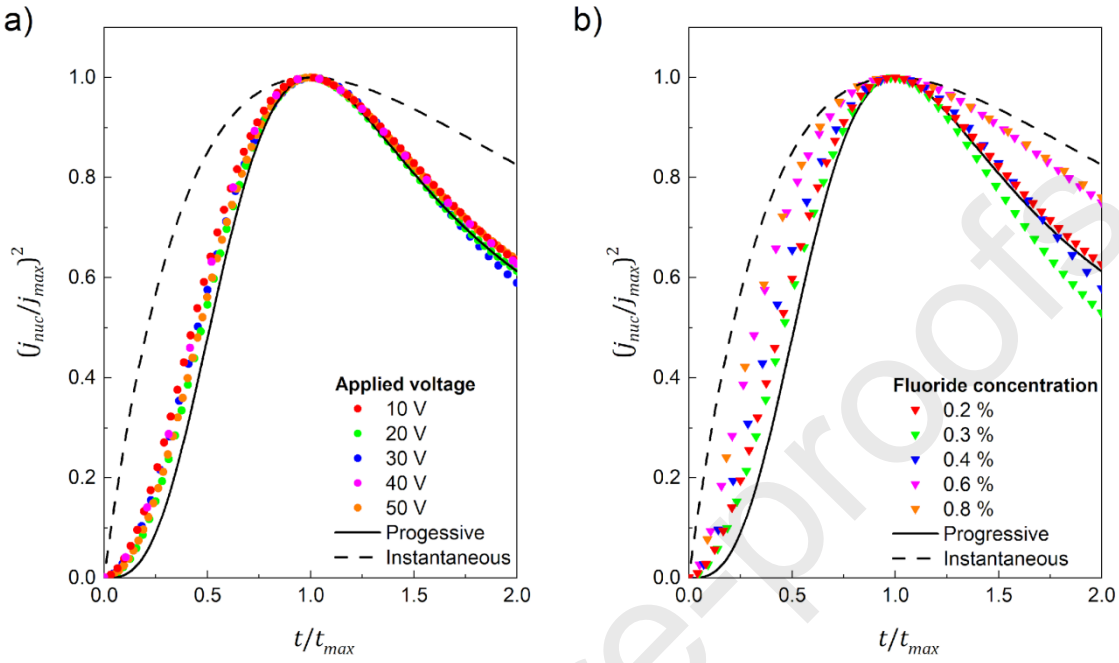

Fig. 8. Non-dimensional $(j_{nuc}/j_{max})^2$ vs t/t_{max} plots for the nucleation current curves extracted from the simulations of the anodization of Ti foils during 6 h at 5 ºC in ethylene glycol-based electrolytes containing 3% V/V water, compared to the instantaneous (– – –) or progressive (——) tridimensional nucleation predictions. a) Applied voltage effect with 0.2% w/V NH_4F. b) Fluoride concentration effect at 40 V.

In summary, experimental j/t profiles as well as the dependence of the pore radius, layer thickness and pore density with anodizing time, are very well described by the proposed model. The evidence indicates that the final morphology features of the NTA-TiO_2 strongly depend on the initial anodization stages, which are related to the oxygen bubble embryos nucleation promoted by the fluoride diffusion inside the film. Accordingly, the position and maximum values in current profiles are accurately described by the nucleation contribution here proposed, which represents the first report that completely describes the overall TiO_2 array growth in terms of physical and chemical parameters (i.e., no fit parameters without physical or chemical meaning were considered). All numerical values obtained for these parameters are consistent and allow describing accurately both current profiles and the main geometrical features of the obtained NTA-TiO_2 arrays for several experimental conditions.

4. Conclusions

Potentiostatic j/t curves recorded during titanium anodization in ethylene glycol-based electrolytes containing fluoride, as well as the surface morphology of the nanotube TiO_2 arrays obtained, show a strong dependence on the experimental conditions employed. The first anodization stages have a key role in the evolution of film nanostructuration, but this complex behavior is not completely described neither by the usually employed FAD nor OBM models. In this regard, we propose a phenomenological model that describes the NTA-TiO_2 growth taking into account the ionic migration in terms of HFM, the electronic current contribution according to the OBM model and the film thinning by chemical dissolution. In addition, the inclusion of the nucleation of oxygen bubbles as the rate determining step at the early anodization stages is considered. For simplicity, we also assume that the nanotubular structure can be approximated to a nanoporous film and no other processes take place during anodization (i.e., nanotube mouth fracture to form nanograss, chemical etching of the initial external layer, and decreasing of ionic conductivity in the oxide). Despite this, by simultaneous fitting of both potentiostatic j/t profiles as well as the time evolution of pore radius, film thickness and pore density for several experimental conditions, the general behavior was accurately described, even for anodization times up to 6 h.

From the present results, it is remarkable that oxide chemical dissolution promoted by the fluoride ions takes place at a non-negligible constant rate independently of the applied voltage, which is a conclusive evidence for a chemical-type instead of field-assisted dissolution process. Also, chemical dissolution is not strong enough to determine the porous nature of the growing film. In addition, fluoride concentration is directly related to the nucleation regimen (i.e., progressive/instantaneous) at early anodization stages, which in turn determines the subsequent film/layer morphology evolution.

As far as we know, this work represents the first report and a novel contribution on the understanding of the mechanisms involved in the growth of nanoporous/nanotubular oxide layers by electrochemical anodization. Further investigations concerning the applicability of this model to an extended set of experimental conditions (anodization temperatures, water content, and solvent nature, among others) will be performed.

Acknowledgements

MIB, WRC and AAC thank CONICET from Argentina for the fellowships granted. We thank the financial support from Project PUE-2017 CONICET #22920170100092, PICT2019-2545 and SECYT-UNC. FESEM and 3D-confocal microscopy facilities at LAMARX, FAMAF-UNC/CONICET, Sistema Nacional de Microscopía - MINCyT, are gratefully acknowledged.

References

[1] H. Bian, Z. Li, J. Pan, F. Lyu, X. Xiao, J. Tang, P. Schmuki, C. Liu, J. Lu, Y. Y. Li, Anodic self-assembly method for synthesizing hierarchical FeS/FeO_x hollow nanospheres, J. Power Sources 484 (2021) 229268.

[2] D. M. Arciniegas Jaimes, P. Márquez, A. Ovalle, J. Escrig, O. Linarez Pérez, N. Bajales, Permalloy nanowires/graphene oxide composite with enhanced conductive properties, Sci. Rep. 10 (2020) 13742.

[3] D. P. Oyarzún, M. López Teijelo, W. Ramos Cervantes, O. E. Linarez Pérez, J. Sánchez, G. del C. Pizzarro, G. Acosta, M. Flores, R. Arratía-Perez, Nanostructuring of anodic copper oxides in fluoride-containing ethylene glycol media, J. Electroanal. Chem. 807 (2017) 181-186.

[4] W. Lee, S. Park, Porous anodic aluminum oxide: Anodization and templated synthesis of functional nanostructures, Chem. Revs. 114 (2014) 7487-7556.

[5] M. I. Broens, W. Ramos Cervantes, D. Oyarzun Jerez, M. López Teijelo, O. E. Linarez Pérez, The keys to avoid undesired structural defects in nanotubular TiO_2 films prepared by electrochemical anodization, Ceram. Int. 46 (2020) 13599-13606.

[6] M. F. Torresan, A. M. Baruzzi, R. A. Iglesias, Enhancing the adsorption of CdSe quantum dots on TiO_2 nanotubes by tuning the solvent polarity, Solar Energy Mater. Solar Cells 164 (2017) 107-113.

[7] T. Yanagishita, H. Hirose, T. Kindo, P. Schmuki, H. Masuda, Fabrication of ideally ordered TiO_2 through-hole membranes by two-layer anodization, RSC Adv. 10 (2020) 37657-37661.

[8] D. Regonini, C. R. Bowen, A. Jaroenworaluck, R. Stevens, A review of growth mechanism, structure and crystallinity of anodized TiO_2 nanotubes, Mater. Sci. Eng. R 74 (2013) 377-406.

[9] P. Roy, S. Berger, P. Schmuki, TiO_2 Nanotubes: Synthesis and Applications, Angew. Chem. Int. Ed. 50 (2011) 2904.

[10] D. Kowalski, D. Kim, P. Schmuki, TiO_2 nanotubes, nanochannels and mesosponge: Self-organized formation and applications, Nano Today 8 (2013) 235 - 264.

[11] M. Paulose, K. Shankar, S. Yoriya, H. E. Prakasam, O. K. Varghese, G. K. Mor, T. A. Latempa, A. Fitzgerald, C. A. Grimes, Anodic Growth of Highly Ordered TiO_2 Nanotube Arrays to 134 μm in Length, J. Phys. Chem. B 110 (2006) 16179-16184.

[12] D. P. Oyarzún, E. C. Muñoz, R. A. Córdova, O. E. Linarez Pérez, R. G. Henríquez, M. López Teijelo, H. Gómez, Morphological, electrochemical and photoelectrochemical characterization of nanotubular TiO_2 synthetized electrochemically from different electrolytes, J. Solid-State Electrochem. 15 (2011) 2265-2275.

[13] D. Regonini, A. Satka, A. Jaroenworaluck, D. W. E. Allsopp, C. R. Bowen, R. Stevens, Factors influencing surface morphology of anodized TiO_2 nanotubes, Electrochim. Acta 74 (2012) 244-253.

[14] X. Zhou, N. T. Nguyen, S. Özkan, P. Schmuki, Anodic TiO_2 nanotube layers: Why does self-organized growth occur – A mini review, Electrochem. Commun. 46 (2014) 157-162.

[15] B. Chong, D. Yu, M. Gao, H. Fan, C. Yang, W. Ma, S. Zhang, X. Zhu, Formation mechanism of gaps and ribs around anodic TiO_2 nanotubes and method to avoid formation of ribs, J. Electrochem. Soc. 162 (2015) H244-H250.

[16] S. Zhang, D. Yu, D.D. Li, Y. Song, J. Che, S. You, X. Zhu, Forming process of anodic TiO_2 nanotubes under a performed compact surface layer, J. Electrochem. Soc. 161 (2014) E135-E141.

[17] B. Chong, D. Yu, R. Jin, Y. Wang, D. Li, Y. Song, M. Gao, X. Zhu, Theoretical derivation of anodizing current and comparison between fitted curves and measured curves under different conditions, Nanotechnology 26 (2015) 145603.

[18] K. Zhang, S. Cao, C. Li, J. Q. L. Jiang, J. Zhang, X. Zhu, Rapid growth of TiO_2 nanotubes under the compact oxide layer: Evidence against the digging manner of dissolution reaction, Electrochem. Comm. 103 (2019) 88-93.

[19] Z. Zhang, Q. Wang, H. Xu, W. Zhang, Q. Zhou, H. Zeng, J. Yang, J. Zhu, X. Zhu, TiO_2 nanotube arrays with a volume expansion factor greater than 2.0: Evidence against the field-assisted ejection theory, Electrochem. Comm. 114 (2020) 106717.

[20] Y. Zhang, H. Fan, X. Ding, Q. Yan, L. Wang, W. Ma, Simulation of anodizing current-time curves and morphology evolution of TiO_2 nanotubes anodized in electrolytes with different NH_4F concentrations, Electrochim. Acta 176 (2015) 1083-1091.

[21] J. Tao, J. Zhao, C. Tang, Y. Kang, Y. Li, Mechanism study of self-organized TiO_2 nanotube arrays by anodization, New J. Chem. 32 (2008) 2164-2168.

[22] G. Butail, P. G. Ganesan, M. Raddiar, R. Teki, N. Ravishankar, D. J. Duquette, G. Ramanath, Kinetics of titania nanotube formation by anodization of titanium films, Thin Solid films 519 (2011) 1821-1824.

[23] D. Kowalski, J. Mallet, J. Michel, M. Molinari, Low electric field strength self-organization of anodic TiO_2 nanotubes in diethylene glycol electrolyte, J. Mater. Chem. A 3 (2015) 6655-6661.

[24] A. Apolinário, P. Quitério, C. T. Sousa, J. Ventura, J. B. Sousa, L. Andrade, A. M. Mendes, J. P. Araújo, Modeling the growth kinetics of anodic TiO_2 nanotubes, J. Phys. Chem. Lett. 6 (2015) 845-851.

[25] X. Li, Y. Zhang, L. Gao, J. Ma, Y. Qiu, X. Xu, J. Ou, W. Ma, The growth rate of nanotubes and the quality of charge during anodization, Electrochem. Comm. 135 (2022) 107184.

[26] T. Gong, C. Li, X. Li, H. Yue, X. Zhu, Z. Zhao, R. Lv, J. Zhu, Evidence of oxygen bubbles forming nanotube embryos in porous anodic oxides, Nanoscale Adv. 3 (2021) 4659-4668.

[27] E. Seçkin, M. Ürgen, A kinetic model for determining morphology transitions and growth kinetics of titania nanotubes during anodization of titanium in ethylene glycol based electrolytes, Surf. Coat. Technol. 409 (2021) 126840.

[28] C. Li, Y. Ni, J. Gong, Y. Song, T. Gong, X. Zhu, A review: research progress on the formation mechanism of porous anodic oxides, Nanoscale Adv. 4 (2022) 322-333.

[29] R. Vargas, D. Carvajal, B. Galavis, A. Maimone, L. Madriz, B. R. Scharifker, High-field growth of semiconducting anodic oxide films on metal surfaces for photocatalytic application, Int. J. Photoenergy (2019) 2571906.

[30] M. I. Broens, W. Ramos Cervantes, A. M. Asenjo Collao, D. P. Oyarzún, M. López Teijelo, O. E. Linarez Pérez, "Nanostructured Seminconducting Oxide Films" (Ch. 3) in "Nanostructured Multifunctional Materials: Synthesis, Characterization, Applications and Computational Simulation". Ed.: E. Franceschini. CRC Press. Taylor and Francis Group. Boca Ratón, EEUU. 2021.

[31] M. J. Dignam, in: J. O'M. Bockris, B. E. Conway, E. Yeager, R. E. White (Eds.), in Comprehensive Treatise of Electrochemistry, vol. 4, Plenum Publishing Corporation, 1981 (Chapter 5).

[32] O. E. Linarez Pérez, V. C. Fuertes, M. A. Pérez, M. López Teijelo, Characterization of the anodic growth and dissolution of oxides films on valve metals, Electrochem. Commun. 10 (2008) 433-437.

[33] J. E. Houser, K. R. Hebert, The role of viscous flow of oxide in the growth of self-ordered porous anodic alumina films, Nat. Mater. 8 (2009) 415-420.

[34] H. Conrad, Thermally activated plastic flow of metals and ceramics with an electric field or current, Mater. Sci. Eng. A 322 (2002) 100-107.

[35] M. Pashchanka, Conceptual progress for explaining and predicting self-organization on anodized aluminum surfaces, Nanomaterials 11 (2021) 2271.

[36] J. Oh, C. V. Thompson, The role of electric field in pore formation during aluminum anodization, Electrochim. Acta 56 (2011) 4044–4051.

[37] W. Huang, H. Xu, Z. Ying, Y. Dan, Q. Zhou, J. Zhang, X. Zhu, Split TiO_2 nanotubes – Evidence of oxygen evolution during Ti anodization, Electrochem. Comm. 106 (2019) 106532.

[38] D. P. Oyarzún, O. E. Linarez Pérez, M. López Teijelo, C. Zúñiga, E. Jeraldo, D. A. Geraldo, R. Arratia-Perez, Atomic force microscopy (AFM) and 3D confocal microscopy as alternative techniques for the morphological characterization of anodic TiO_2 nanoporous layers, Mater. Lett. 165 (2016) 67-70.

[39] P. J. Boddy, Oxygen Evolution on Semiconducting TiO_2, J. Electrochem. Soc 115 (1968) 199-203.

[40] M. A. Abdel Rahim, Variation of the dielectric constant of anodic oxide films on titanium with oxygen evolution, J. Appl. Electrochem. 25 (1995) 881-885.

[41] S. Berger, J. Kunze, P. Schmuki, D. LeClere, A. T. Valota, P. Skeldon, G. E. Thompson, A lithographic approach to determine volume expansion factors during anodization: Using the example of initiation and growth of TiO_2-nanotubes, Electrochim. Acta 54 (2009) 5942-5948.

[42] J. Naduvath, P. Bhargava, S. Mallick, Mechanism of titania nanograss formation during anodization, Chem. Phys. Lett. 626 (2015) 15-19.

[43] M. Palomar-Pardavé, M. Romero-Romo, M. T. Ramírez-Silva, J. Mostany, B. R. Scharifker, Gathering kinetic data of electrochemical phase formation processes trough analysis of experimental current transients. Overview and new approaches, ECS Transactions 3 (2007) 45-52.

[44] O. E. Linarez Pérez, M. D. Sánchez, M. López Teijelo, Characterization of growth of anodic antimony oxide films by ellipsometry and XPS, J. Electroanal. Chem. 645 (2010) 143-148.

[45] S. Ikonopisov, Theory of electrical breakdown during formation of barrier anodic films, Electrochim. Acta 22 (1977) 1077-1082.

[46] J. M. Albella, I. Montero, J. M. Martínez-Duart, A theory of avalanche breakdown during anodic oxidation, Electrochim. Acta 32 (1987) 255-258.

[47] B. Scharifker, G. Hills, Theoretical and experimental studies of multiple nucleation, Electrochim. Acta 28 (1983) 879-889.

[48] B. R. Scharifker, J. Monstany, Three-dimensional nucleation with diffusion controlled growth. Part I. Number density of active sites and nucleation rates per site, J. Electroanal. Chem. 177 (1984) 13-23.

[49] B. R. Scharifker, Diffusion to ensembles of microeletrodes, J. Electroanal. Chem. 240 (1988) 61-76.

[50] B. A. Berg, S. Dubey, Finite Volume Kolmogorov-Johnson-Mehl-Avrami theory, Phys. Rev. Lett. 100 (2008) 165702.

[51] J. M. Macak, H. Hildebrand, U. Marten-Jahns, P. Schmuki, Mechanistic aspects and growth of large diameter self-organized TiO_2 nanotubes, J. Electroanal. Chem. 621 (2008) 254-266.

[52] S. P. Albu, P. Schmuki, Influence of anodization parameters on the expansion factor of TiO_2 nanotubes, Electrochim. Acta 91 (2013) 90-95.

[53] D. R. Lide (Ed.), Handbook of Chemistry and Physics, 85th ed., CRC Press, Boca Raton, 2005.

[54] G. G. Marmitt, S. K. Nandi, D. K. Venkatachalam, R. G. Elliam, M. Vos, P. L. Grande, Oxygen diffusion in TiO_2 films studied by electron and ion Rutherford backscattering, Thin Solid Films 629 (2017) 97-102.

[55] M. Yashima, T. Tsujiguchi, K. Fujii, E. Niwa, S. Nishioka, J. R. Hester, K. Maeda, Direct evidence for two-dimensional oxide-ion diffusion in the hexagonal perovskite-related oxide $Ba_3MoNbO_{8.5-\delta}$, J. Mater. Chem. A. 7 (2019) 13910-13916.

[56] M. Kessel, R. A. De Souza, M. Martin, Oxygen diffusion in single crystal barium titanate, Phys. Chem. Chem. Phys. 17 (2015) 12587-12597.

Table 1. Fitted parameters obtained for the anodization of Ti foils at 5ºC during 6 h in ethylene glycol + 3% V/V water electrolytes.

	$10^8 \times A$ /A cm^{-2}	$10^6 \times \beta$ /cm V^{-1}	j_{dis} /μA cm^{-2}	$j_{e,o}$ /μA cm^{-2}	$10^{-5} \times \alpha$ /cm^{-1}	υ_{nuc} /s^{-1}	$10^{-9} \times N_{max}$ /cm^{-2}	υ_{coal} /s^{-1}	$10^{-9} \times \eta N_{max}$ /cm^{-2}	$10^{13} \times Dc_F$ /mol cm^{-1} s^{-1}	$10^8 \times \sigma$ /cm s^{-1}
a) $c(NH_4F)$ = 0.2 % w/V											
E /V											
10	1.32	2.8	78	0.7	1.0	6×10^{-7}	17	3×10^{-7}	4.4	8×10^{-2}	0.8
20	1.10	3.1	85	1.3	0.8	1×10^{-6}	13	6×10^{-7}	4.1	5×10^{-2}	1.1
30	1.51	3.3	79	4.2	1.6	4×10^{-6}	10	1×10^{-6}	3.5	0.1	1.4
40	1.34	3.0	96	8.3	2.2	5×10^{-5}	8.2	5×10^{-5}	3.1	0.7	1.6
50	2.67	2.8	87	9.5	1.1	2×10^{-5}	9.2	4×10^{-6}	2.8	3.6	2.3
b) E = 40V											
$c(NH_4F)$ /% w/V											
0.2	1.34	3.0	96	8.3	2.2	5×10^{-5}	8.2	5×10^{-5}	3.1	0.7	1.6
0.4	1.25	3.1	153	9.8	1.1	3×10^{-3}	9.2	1×10^{-4}	3.7	4.2	1.9
0.6	1.10	2.9	176	17.3	1.3	0.2	14	2×10^{-4}	7	15	2.3
0.8	1.04	3.3	222	26.1	0.9	1.6	26	7×10^{-4}	17	62	2.8

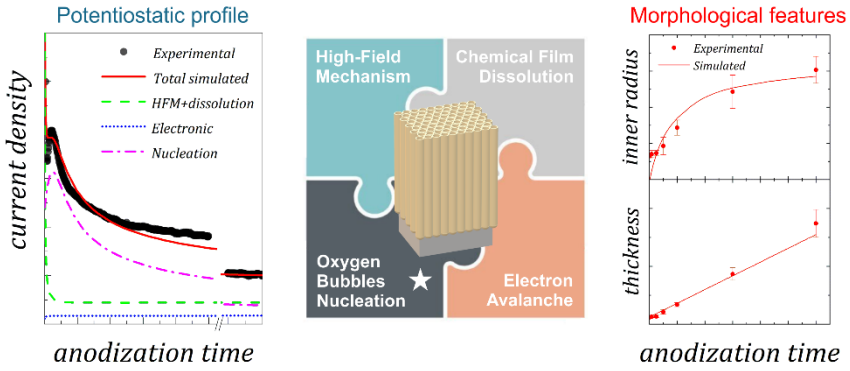

Highlights:

- A phenomenological model for anodic growth of TiO_2 nanotube arrays is developed
- Nucleation of O_2 bubbles is the porous layer initiation step
- First anodization stages play a key role in the evolution of oxide nanostructuration
- Oxide layer dissolution is not a field activated process
- Simultaneous fitting of *j/t* profiles and morphological layer features were described

Martín I. Broens: Conceptualization, Investigation, Data curation, Writing- Original draft preparation. **Wilkendry Ramos Cervantes:** Conceptualization, Investigation, Data curation, Writing- Original draft preparation. **Andres M. Asenjo Collao**: Conceptualization, Investigation, Data curation, Writing- Original draft preparation. **Rodrigo A. Iglesias**: Investigation, Writing - Reviewing & Editing, Resources. **Manuel López Teijelo:** Writing- Reviewing and Editing, Resources. **Omar E. Linarez Pérez**: Supervision, Writing- Reviewing and Editing, Resources.